Longitudinal and Lateral Spectra of Turbulence in the Atmospheric Boundary Layer at the Kennedy Space Center[1]

GEORGE H. FICHTL

Aerospace Environment Division, NASA-George C. Marshall Space Flight Center, Huntsville, Ala.

AND GEORGE E. McVEHIL[2]

Cornell Aeronautical Lab., Inc., Buffalo, N. Y.

(Manuscript received 8 July 1969, in revised form 22 September 1969)

An engineering spectral model of turbulence is developed with horizontal wind observations obtained at the NASA 150-m meteorological tower at Cape Kennedy, Fla. Spectra, measured at six levels, are collapsed at each level with $[nS(n)/u_{*0}^2, f]$-coordinates, where $S(n)$ is the longitudinal or lateral spectral energy density at frequency n (Hz), u_{*0} the surface friction velocity, and $f=nz/\bar{u}$, $\bar{u}$ being the mean wind speed at height z. A vertical collapse of the dimensionless spectra is produced by assuming they are shape-invariant in the vertical.

An analysis of the longitudinal spectrum in the inertial subrange, at the 18-m level, implies that the local mechanical and buoyant production rates of turbulent kinetic energy are balanced by the local dissipation and energy flux divergence, respectively.

1. Introduction

To determine the response of space vehicles, aircraft, tall structures, etc., to atmospheric turbulence, the engineer requires specific information about the spectral nature of atmospheric turbulence because the equations of motion of these vehicles or structures are linear and are solved with Fourier transform techniques. Thus, the environmental forcing functions must be represented in terms of spectra. Motivated by this requirement, we have developed a model for the longitudinal and lateral spectra of turbulence for the Kennedy Space Center (KSC) area. The longitudinal and lateral components of turbulence are the wind fluctuations parallel and normal to the mean wind vector.

2. The NASA 150-m meteorological tower site

To obtain micrometeorological data representative of the Cape Kennedy area, especially in the vicinity of the Apollo/Saturn V launch pads, a 150-m meteorological tower was constructed on Merritt Island at KSC. The tower facility, discussed in detail in a report by Kaufman and Keene (1965), is only briefly described here.

Fig. 1 shows the location of the facility with respect to the Saturn V space vehicle launch complex 39. Located about 5 km from the Atlantic Ocean, the tower is situated in a well-exposed area free of near-by structures which could interfere with the air flow.

The aerial photograph (Fig. 2) of the terrain surrounding the tower (point T) was taken at 1200 MSL. In the quadrant from approximately 300° north azimuth with respect to the tower, clockwise around to 90°, the terrain is homogeneous and is covered with vegetation ~1–2 m high. Another homogeneous fetch with the same type of vegetation occurs in the 135–160° quadrant. The areas A (230–300°), B (90–135°), and C (160–180°) are covered with trees from ~10–15 m tall. The fetch from the tower to areas A or C is ~200 m, and the fetch to area B ~450 m. The vegetation over these fetches is similar to that in the area to the north of the tower. To the south-southwest in the 180–230° quadrant, 225 m from the tower, there is a body of water called Happy Creek.

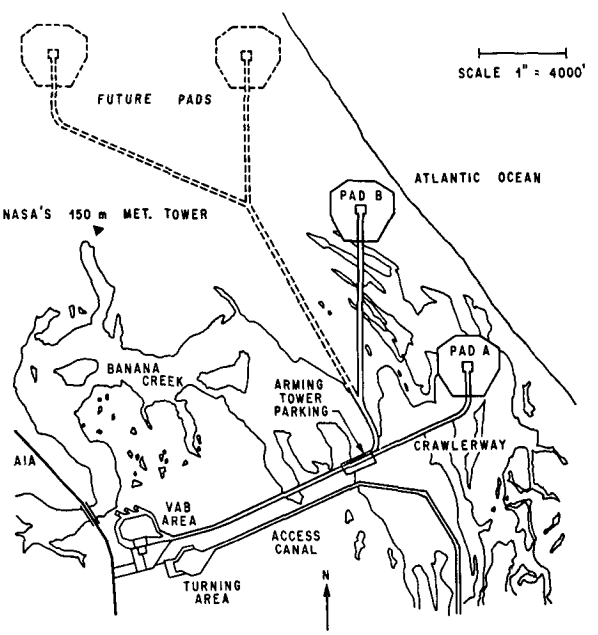

FIG. 1. NASA Launch Complex 39, Kennedy Space Center, Fla.

[1] Presented at the AGARD Specialists Meeting on The Aerodynamics of Atmospheric Shear Flows, Munich, 15–17 September 1969.

[2] Present affiliation: EG & G, Inc., Environmental Services Operation, Boulder, Colo.

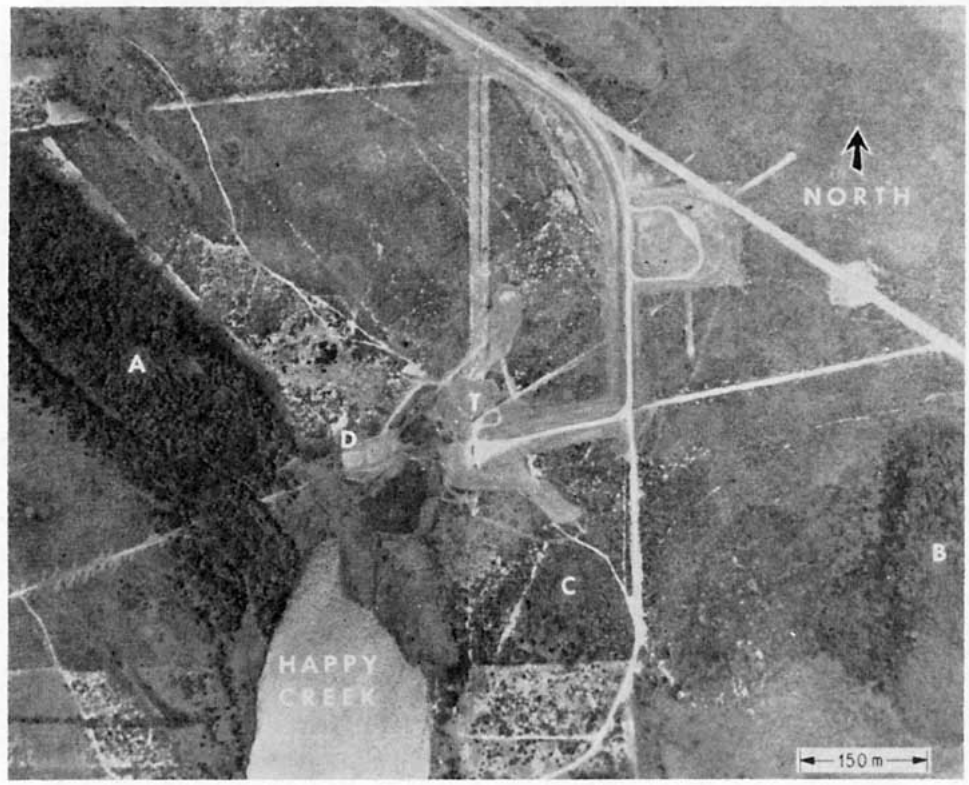

FIG. 2. Aerial plane view of the terrain surrounding the NASA 150-m meteorological tower.

The complete tower facility comprises two towers, one 18 m and the other 150 m high (see Fig. 3). The levels on both towers are instrumented with Climet (Model C1-14) wind sensors. Temperature sensors, Climet (Model C1-016) aspirated thermocouples, are located at the 3- and 18-m levels on the small tower and at the 30-, 60-, 120- and 150- m levels on the large tower. Foxboro (Model F-2711AG) dew-point temperature sensors are located at the 60- and 150-m levels on the large tower and at the 3-m level on the 18-m tower. Wind speed and direction data can be recorded on both paper strip charts and analog magnetic tapes with an Ampex FR-1200 fourteen-channel magnetic tape recorder which uses a 14-inch reel. The temperature and dew-point data are recorded on paper strip charts. To avoid tower interference of the flow, the large tower is instrumented with two banks of wind sensors. The details of how and when one switches from one bank of instrumentation to the other bank is discussed by Kaufman and Keene (1965). During a test in which the wind data are stored on analog tape, only one bank of instrumentation is used to avoid interruption of the wind data signals within any recording period to avoid data processing difficulties when converting analog tapes to digital tapes.

In an earlier report, Fichtl (1968) discussed the surface roughness length configuration associated with the NASA meteorological tower. This analysis was based on wind profile laws that are consistent with the Monin-Obukhov similarity hypothesis. The calculations of z_0 were based on wind data obtained at the 18- and

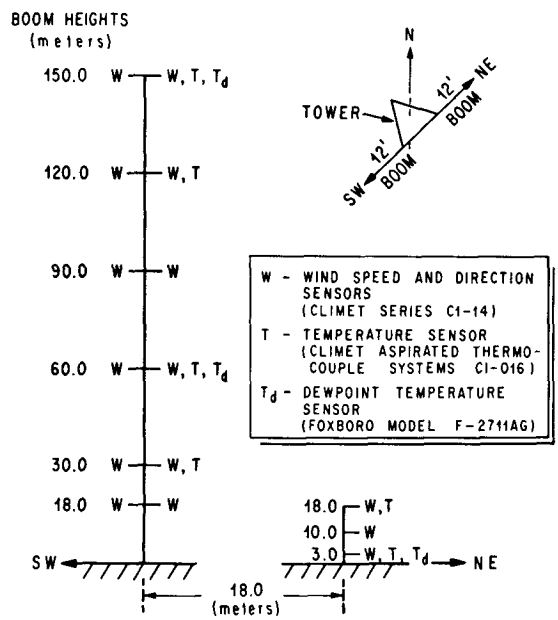

FIG. 3. Schematic diagram of the location of instrumentation on the NASA 150-m meteorological tower at Kennedy Space Center. The tower is at point T. See text for descriptions of areas A, B, C.

30-m levels and on temperature data obtained at the 18- and 60-m levels. Most of the measurements were obtained during the hours of 0700 and 1600 EST; the gradient Richardson numbers at 23 m (geometric mean height between 18 and 30 m) for the 39 cases ranged between −5.8 and +0.08. The results of these calculations (see Fig. 4) show the effect the terrain features have upon the surface roughness. Later, it will be shown, through an analysis of the energy budget at 18 m, that these roughness lengths are too large.

3. Computations and initial scaling

To establish a spectral model of turbulence for KSC approximately 50 cases of turbulence were analyzed. Each case consisted of 1-hr time histories of wind speed and direction measured at the 18-, 30-, 60-, 90-, 120- and 150-m levels. The procedure used to calculate the longitudinal and lateral components of turbulence consisted of 1) converting the digitized wind speeds and directions (10 data points per second) into the associated north-south and east-west components and averaging these components over the duration time of each test; 2) calculating the mean wind speed and direction with the averaged components; 3) projecting the original digitized data onto the mean wind vector and subtracting the mean wind speed to yield the longitudinal components of turbulence; and 4) projecting the original digitized data onto a normal-to-the-mean-wind vector to obtain the lateral components of turbulence. Trends contained within the data were removed by fitting the longitudinal and lateral components of turbulence to second-order polynomials and, in turn, subtracting these polynomials from the component time histories. To reduce computation time, the data, with trend removed, were block-averaged over half-second intervals. The longitudinal and lateral spectra were calculated by using the standard correlation Fourier transform methods given by Blackman and Tukey (1958). These spectra were corrected for the half-second block-averaging operation with the procedure given by Pasquill (1962) and for the response properties of the instrumentation.

To combine the spectra for each level on the tower, it was assumed that the similarity theory of Monin (1959) for the vertical velocity spectrum could be applied to the longitudinal and lateral spectra, so that

$$\frac{nS(n)}{u_{*0}^2}=F(f,\mathrm{Ri}), \tag{1}$$

where $nS(n)$ is the logarithmic longitudinal or lateral spectrum associated with frequency n(Hz), and u_{*0} is the surface friction velocity, or rather, the square root of the tangential eddy stress per unit mass. F is tentatively a universal function of the dimensionless wavenumber f and the gradient Richardson number Ri.

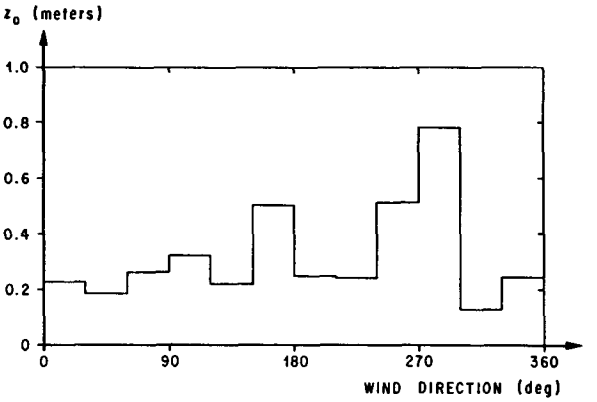

FIG. 4. Tentative azimuthal distribution of the surface roughness length at the NASA 150-m meteorological tower site.

The dimensionless wavenumber is given by

$$f=\frac{nz}{\bar{u}(z)}. \tag{2}$$

Since the tower did not have the capability to measure vertical velocity fluctuations, the Reynolds stress, and hence u_*^2, cannot be calculated with first principles; viz., $u_*^2=\overline{u'w'}$, where u' and w' are the longitudinal and vertical velocity fluctuations and the overbar denotes a time-averaging operator. However, an estimate of the surface friction velocity can be calculated from mean wind and temperature profile data.

According to Lumley and Panofsky (1964), the mean wind profile in approximately the first 30 m of the atmosphere is given by

$$\bar{u}(z)=\frac{u_{*0}}{k_1}\left[\ln\frac{z}{z_0}-\psi(z/L')\right], \tag{3}$$

where k_1 is von Kármán's constant with numerical value approximately equal to 0.4, and ψ is a universal function of z/L', L' being a stability length given by

$$L'=u_{*0}\left(\frac{d\bar{u}}{dz}\right)\bar{T}\Big/\left[k_1 g\left(\frac{d\bar{\theta}}{dz}\right)\right], \tag{4}$$

where $\bar{T}$ and $\bar{\theta}$ are the Kelvin and potential temperatures associated with the mean flow. The quantity z/L' is related to the gradient Richardson number

$$\mathrm{Ri}=\frac{g}{\bar{\theta}}\left(\frac{d\bar{\theta}}{dz}\right)\Big/\left(\frac{d\bar{u}}{dz}\right)^2, \tag{5}$$

through the relationships

$$z/L'=\frac{\mathrm{Ri}}{(1-18\mathrm{Ri})^{\frac{1}{2}}}, \quad (\mathrm{Ri}<-0.01), \tag{6}$$

$$z/L'=\mathrm{Ri}, \quad (-0.01\leqq\mathrm{Ri}\leqq 0.01), \tag{7}$$

$$z/L'=\frac{\mathrm{Ri}}{1-7\mathrm{Ri}}, \quad (0.1\geqq \mathrm{Ri}>0.01). \tag{8}$$

Eq. (6) is a form of the KEYPS (Lumley and Panofsky, 1964) equation. The functions $\psi(z/L')$ associated with (7) and (8) are given by

$$\psi(z/L')=-4.5\frac{z}{L'}, \quad (-0.01\leqq \mathrm{Ri}\leqq 0.01), \tag{9}$$

$$\psi(z/L')=-7\frac{z}{L'}, \quad (0.1\geqq \mathrm{Ri}>0.01). \tag{10}$$

Lumley and Panofsky (1964) have graphically indicated the function $\psi(z/L')$ for $\mathrm{Ri}<-0.01$ and the form

$$\psi(z/L')=0.044\left(\frac{-z/L'}{0.01}\right)^{1.0674-0.679\ \ln(-z/L'/0.01)}, \quad (\mathrm{Ri}<-0.01) \tag{11}$$

faithfully reproduces their curve.

The calculation of u_{*0} was based upon the wind data measured at the 18- and 30-m levels and the temperature data measured at the 18- and 60-m levels. An estimate of the gradient Richardson number (5) at the 23-m level was determined by assuming that the mean wind speed and temperature are logarithmically distributed between these levels. The gradient Richardson number estimated in this manner is given by

$$\mathrm{Ri}(z_g)=\frac{g}{\bar{T}(z_g)}\left[\frac{\bar{T}(z_2)-\bar{T}(z_1)}{z_g\ln(z_2/z_1)}+\frac{g}{C_p}\right]\left[\frac{\bar{u}(z_2)-\bar{u}(z_1)}{z_g\ln(z_2/z_1)}\right]^{-2}, \tag{12}$$

where $\bar{T}(z)$ is the mean temperature at height z; z_1 and z_2 denote 18 and 30 m; and $z_g=\sqrt{z_1z_2}$.

To calculate u_{*0}, z_g/L' was evaluated for each case by means of one of the three equations (6)–(8), corresponding to the appropriate Richardson number class. L' was then assumed to be invariant with height, and $\psi(18/L')$ was estimated by Eqs. (9)–(11). Eq. (3) was then evaluated at the 18-m level and solved to yield u_{*0}. The values of z_0 used for this calculation are given in Fig. 4.

4. The inertial subrange and revised values of the surface roughness lengths

In the inertial subrange the longitudinal spectrum is given by

$$\frac{nS_u(n)}{u_{*0}^2}=\alpha k_1^{-\frac{2}{3}}\phi_\epsilon^{\frac{2}{3}}f^{-\frac{2}{3}}, \tag{13}$$

where α is Kolomogorov's constant with numerical value equal to 0.146 according to Record and Cramer (1966). The quantity ϕ_ϵ is the dimensionless dissipation rate of turbulent kinetic energy per unit mass given by

$$\phi_\epsilon=\frac{k_1z\epsilon}{u_{*0}^3}, \tag{14}$$

where ϵ is the rate of dissipation of turbulent energy. Below 30 m, where we should expect the Monin and Obukhov similarity hypothesis for the wind profile to be valid, ϕ_ϵ is a function of Ri only.

Inferences concerning the dependence of ϕ_ϵ on Ri can be made with the aid of the eddy energy equation. For homogeneous terrain, this equation is given by

$$\frac{d\overline{E'}}{dt}=u_*^2\frac{d\bar{u}}{dz}+\frac{H}{C_p\rho}\frac{g}{\bar{T}}-\epsilon-\frac{d}{dz}\left(\frac{\overline{p'w'}}{\rho}+\overline{w'E'}\right), \tag{15}$$

where $H/(C_p\rho)$ is the eddy heat flux $\overline{\theta'w'}$, ρ the mean density, E' the turbulent kinetic energy per unit mass, p' and w' denote the turbulent fluctuations of pressure and vertical velocity, and u_* is the local friction velocity ($u_*=u_{*0}$ in the Monin layer). Following Busch and Panofsky (1968), we write (15) in dimensionless form, so that

$$\left(\frac{k_1z}{u_{*0}^3}\right)\frac{d\overline{E'}}{dt}=(u_*/u_{*0})^2\phi-\frac{z}{L}-\phi_\epsilon-\phi_D. \tag{16}$$

The terms in this expression are in one-to-one correspondence with those of (15) and L is the Monin-Obukhov stability length

$$L=-\frac{u_{*0}^3C_p\rho\bar{T}}{k_1gH}. \tag{17}$$

Near the ground a majority of meteorological conditions are characterized, at least approximately, by horizontal homogeneity, steady mean wind with no change of wind direction with height, and steady heating from below. In most cases, it is reasonable to make these assumptions with regard to the KSC tower site. Thus, to a reasonable degree of approximation, we have $d\overline{E'}/dt=0$, and Eq. (16) implies that in the Monin layer

$$\phi-\frac{z}{L}-\phi_\epsilon-\phi_D=0. \tag{18}$$

Various authors have hypothesized schemes to balance the left-hand side of (18). Lumley and Panofsky (1964) suggest that the local mechanical energy production is balanced by the local viscous dissipation, so that

$$\phi_\epsilon=\phi, \tag{19}$$

and thus the buoyant energy production is balanced by the energy flux divergence term, making

$$\phi_D=-z/L. \tag{20}$$

Busch and Panofsky (1968) suggest that the flux divergence term is negligible and the local viscous dissipation is balanced by both the local mechanical and buoyant energy productions, so that

$$\phi_\epsilon=\phi-z/L. \tag{21}$$

We shall call (19) and (21) hypotheses I and II, respectively.

According to Lumley and Panofsky,

$$\phi=(1-18\mathrm{Ri})^{-\frac{1}{4}} \tag{22}$$

in the unstable Monin layer. This form of the dimensionless shear is consistent with (6). Upon combining (13), (19) and (22), the specturm in the Kolmogorov subrange for hypothesis I takes the form

$$\left[\frac{nS_u(n)}{u_{*0}^2}\right]_{\mathrm{I}}=\alpha k_1^{-\frac{2}{3}}(1-18\mathrm{Ri})^{-1/6}f^{-\frac{2}{3}}. \tag{23}$$

Combining (6), (13), (17), (21) and (22) yields

$$\left[\frac{nS_u(n)}{u_{*0}^2}\right]_{\mathrm{II}}=\alpha k_1^{-\frac{2}{3}}\left[\frac{1-\mathrm{Ri}K_m/K_h}{(1-18\mathrm{Ri})^{\frac{1}{4}}}\right]^{\frac{2}{3}}f^{-\frac{2}{3}} \tag{24}$$

for hypothesis II, where K_m and K_h are the eddy viscosity and heat conduction coefficients given by

$$K_m=u_*^2\Big/\frac{d\bar{u}}{dz}, \tag{25}$$

$$K_h=-H\Big/\left(C_p\rho\frac{d\bar{\theta}}{dz}\right). \tag{26}$$

Fig. 5 illustrates $[nS_u(n)/u_{*0}^2]_{\mathrm{I}}$ and $[nS_u(n)/u_{*0}^2]_{\mathrm{II}}$ as functions of $-\mathrm{Ri}$ for $f=1.0$ and $K_h/K_m=1.3$. As $-\mathrm{Ri}$ approaches zero, $[nS_u(n)/u_{*0}^2]_{\mathrm{I}}$ approaches $[nS_u(n)/u_{*0}^2]_{\mathrm{II}}$. The difference between $[S_u]_{\mathrm{I}}$ and $[S_u]_{\mathrm{II}}$ is small (within the noise level of the data) for $\mathrm{Ri}>-1.0$, and

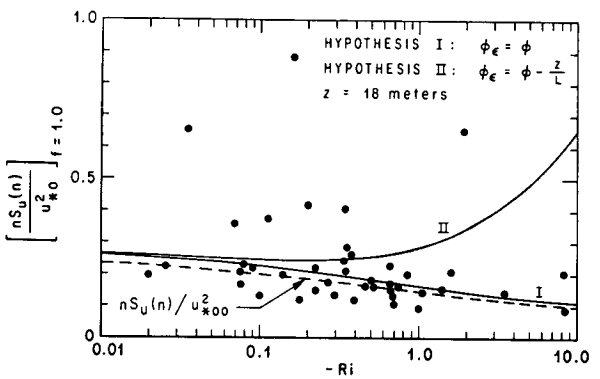

FIG. 5. The dimensionless logarithmic longitudinal spectrum at $f=1.0$ and $z=18$ m as a function of $-\mathrm{Ri}$. The variations of $[nS_u(n)/u_{*0}^2]_{f=1.0}$ for hypotheses I and II are indicated. The dashed curve corresponds to $[nS_u(n)/u_{*00}^2]_{f=1.0}$ with $z_0=0.18$ m and $z_{00}=0.23$ m for a type I energy budget.

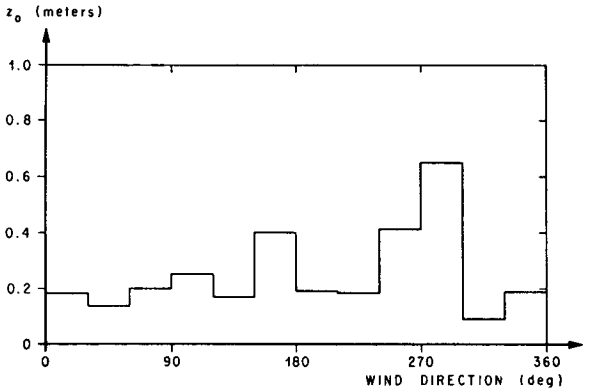

FIG. 6. Revised azimuthal distribution of the surface roughness length based upon energy budget considerations at $z=18$ m.

thus it is difficult to reject one hypothesis in favor of the other for sufficiently small $-\mathrm{Ri}$.

The 18-m level, longitudinal spectra were used to test hypotheses I and II. At 18 m the cut-off value of f was ~ 2.0 in most of the cases. Actually, the Kolmogorov subrange occurs at much greater dimensionless wavenumbers; however, the $-5/3$ power law behavior extends down to values of f on the order of unity for the longitudinal spectrum, while this is not true for the lateral spectrum. In addition, the Monin and Obukhov similarity hypothesis for the wind profile, the basis for the calculation of u_{*0} is, at most, valid below 30 m. Accordingly, the 18-m longitudinal spectra are the only ones that could be used to test the validity of hypotheses I and II without introducing assumptions about how the eddy stress and heat flux vary with height.

In Fig. 5 we have plotted the experimental values of $nS_u(n)/u_{*0}^2$ for the longitudinal spectrum for $f=1.0$ as a function of $-\mathrm{Ri}$ .The experimental results scatter about the dashed line, but they appear to favor hypothesis I more than hypothesis II, especially for $\mathrm{Ri}\leqq -3.0$. If we accept hypothesis I, then we must conclude that the scaling velocities u_{*0} are too large and thus the roughness lengths are too large. If we reject hypothesis I, then we must accept a more complicated energy balance system. We shall invoke Occam's razor and accept hypothesis I and correct the surface roughness lengths.

We denote the surface roughness lengths in Fig. 4 with z_{00}, and the correct ones resulting from the analysis of the longitudinal spectrum will be denoted with z_0. The corresponding friction velocities will be denoted by u_{*00} and u_{*0}, respectively. The longitudinal spectrum in the inertial subrange, scaled in terms of u_{*00}, is given by

$$\frac{nS_u(n)}{u_{*00}^2}=\left[\left(\ln\frac{z}{z_{00}}-\psi(\mathrm{Ri})\right)\Big/\left(\ln\frac{z}{z_0}-\psi(\mathrm{Ri})\right)\right]^2 \times\alpha k_1^{-\frac{2}{3}}(1-18\mathrm{Ri})^{-1/6}f^{-\frac{2}{3}}. \tag{27}$$

The data points in Fig. 5 correspond to $nS_u(n)/u_{*00}^2$,

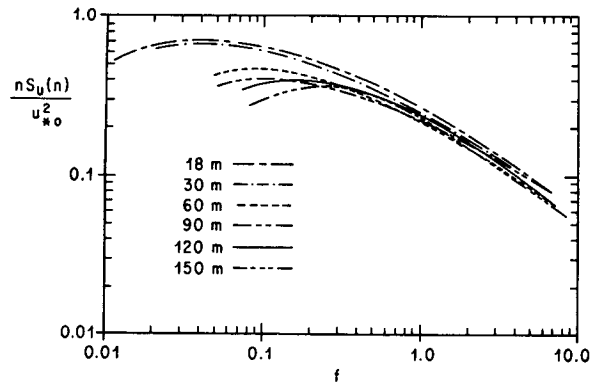

FIG. 7. Dimensionless logarithmic longitudinal spectra for neutral wind conditions.

not $nS_u(n)/u_{*0}^2$. At neutral stability (Ri=0), we have $\psi(0)=0$, and (27) reduces to

$$\left[\ln\frac{z}{z_{00}}\Big/\ln\frac{z}{z_0}\right]^2=\frac{nS_u(n)k_1^{\frac{2}{3}}}{u_{*00}^2\alpha} \tag{28}$$

for $f=1.0$. Denoting the right-hand side of (28) by χ^{-2} and solving for z_0, we find

$$z_0=z^{1-\chi}z_{00}^{\chi}. \tag{29}$$

Upon extrapolating the data in Fig. 5 to Ri=0 at $f=1$, we find $nS_u(n)/u_{*00}^2=0.24$, so that $\chi=1.059$. The new values of z_0 for this value of χ and $z=18$ m are shown in Fig. 6. Substitution of (29) into (27) yields

$$\frac{nS_u(n)}{u_{*00}^2}=\left[\left(\chi^{-1}\ln\frac{z}{z_0}-\psi(\mathrm{Ri})\right)\Big/\left(\ln\frac{z}{z_0}-\psi(\mathrm{Ri})\right)\right]^2 \alpha k_1^{-\frac{2}{3}}(1-18\mathrm{Ri})^{-1/6}f^{-\frac{2}{3}}. \tag{30}$$

The dashed curve in Fig. 5 represents $nS_u(n)/u_{*00}^2$ as a function of $-$Ri according to (30) for $\chi=1.059$ and $z_0=0.18$ m ($z_{00}=0.23$ m), and it appears to fit the data reasonably well. The function $[nS_u(n)/u_{*00}^2]_{f=1.0}$ for the range of variation of z_0 illustrated in Fig. 6 departs from the dashed curve by only a few tenths of one per cent. This means a spectral model of the longitudinal and lateral components of turbulence can be developed in terms of u_{*00}, and the final results can be corrected by applying a multiplicative factor which is a function of the Richardson number and a nominal roughness length for the site.

5. Extrapolation to neutral wind conditions (Ri=0)

The meteorological conditions of particular engineering interest are those associated with mean wind speeds at the 18-m level greater than approximately 10 m sec^{-1}. During these flow conditions, the boundary layer is well mixed so that vertical gradients of the mean flow entropy and thus potential temperature are small and the wind shears are large. Thus, the Richardson number vanishes or at least becomes very small. Accordingly, the neutral longitudinal and lateral spectra are of particular interest in the design and operation of space vehicles. The neutral spectra were determined by extrapolating the data to Ri=0 by the procedure developed by Berman (1965). Scaled spectra $nS(n)/u_{*00}^2$ were plotted vs Ri for various values of f, and curves were drawn by eye. Of course, the data points scattered about this line. The values of $nS(n)/u_{*00}^2$ at Ri=0 were then read off and corrected by multiplying the results by χ^2 to yield the neutral spectra $nS(n)/u_{*0}^2$ for the various levels on the tower. The results of this graphical process are shown in Figs. 7 and 8 where the positions of the maxima shift toward higher values of f as the height increases. This means that Monin coordinates $[nS(n)/u_{*0}^2,f]$ fail to collapse the spectra in the vertical so that $F(f, \mathrm{Ri})$ is not a universal function, and thus an added height dependence should be included in the analysis. Busch and Panofsky have obtained similar results from analyses of tower data from Round Hill. The failure of the Monin coordinates to collapse the spectra in the vertical can be attributed to vertical variations in both the Reynolds stress and the length scale used to scale the wavenumber $n/\bar{u}(z)$.

Above the Monin layer ($z<30$ m) in the Ekman layer ($z>30$ m), the tangential Reynolds stress decreases with height. In addition, the variances of the longitudinal and lateral components of turbulence are decreasing functions of z. Thus, if u_* is the correct scaling velocity, scaling the spectra with the surface value of the friction velocity will cause the scaled spectra at the upper levels to fall below the 18-m spectra.

By scaling the wavenumber with z, we have assumed that the integral scales of the longitudinal and lateral components of turbulence are proportional to z. One might suspect from the behavior of eddy coefficients (Blackadar *et al.*, 1965) that, if the local integral scales have vertical variations, then they should increase at a rate slower than z. In addition, we have no knowledge that the integral scales of the longitudinal and lateral spectra should have the same vertical variation. How-

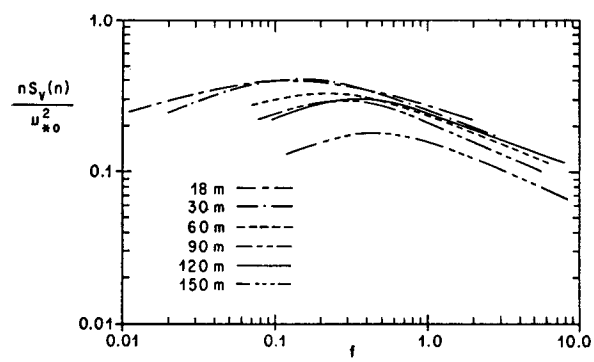

FIG. 8. Dimensionless logarithmic lateral spectra for neutral wind conditions.

ever, the analysis did show that Monin coordinates will collapse spectra associated with various turbulence intensities at any particular level in the vertical.

To produce a vertical collapse of the data, it was assumed, for engineering purposes, that the spectra in Monin coordinates are shape-invariant in the vertical. This hypothesis appears to be reasonable and permits a practical approach to developing an engineering spectral model of turbulence.

The vertical variation of the dimensionless wavenumber f_{mu} associated with the peak of the logarithmic spectrum scaled in Monin coordinates is given in Fig. 9. A least-squares analysis of the data in this figure yielded the result

$$f_{mu}=0.03(z/18), \tag{31}$$

where z is in meters. A plot of $nS_u(n)/u_{*0}^2$ vs f/f_{mu} will shift the spectra at the various levels so that all the peaks of the logarithmic longitudinal spectra are located at $f/f_{mu}=1$. Values of f_{mu} from other tower sites are indicated in Fig. 9.

The average ratio β_u of the shifted spectrum at level z and the 18-m spectrum, $[S_u(f/f_{mu},z)/S_u(f/f_{mu},18)]$, is shown in Fig. 10. A least-squares analysis of these data yielded the result

$$\beta_u=(z/18)^{-0.63}, \tag{32}$$

where z is in meters. A plot $nS_u(n)/\beta_u u_{*0}^2$ vs f/f_{mu} will collapse the longitudinal spectra. The collapsed longitudinal data are plotted as a function of $0.03\ f/f_{mu}$ in Fig. 11.

The function

$$\frac{nS_u(n)}{\beta_u u_{*0}^2}=\frac{C_u f/f_{mu}}{[1+1.5(f/f_{mu})^{r_u}]^{5/3r_u}} \tag{33}$$

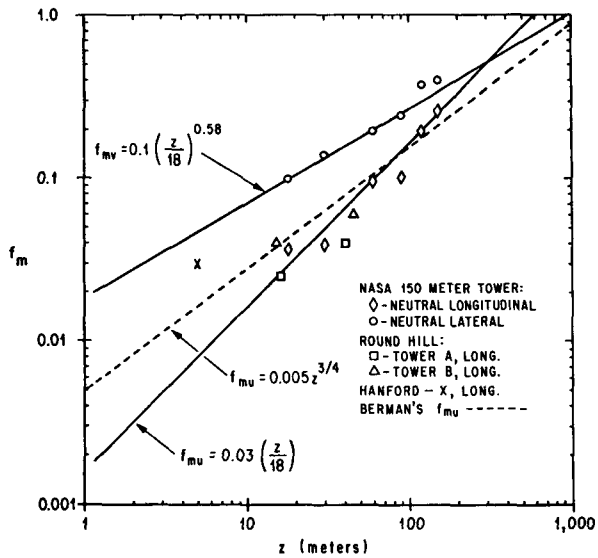

FIG. 9. Vertical distributions of the dimensionless frequencies f_{mu} and f_{mv} associated with the peaks of the logarithmic longitudinal and lateral spectra for neutral stability conditions.

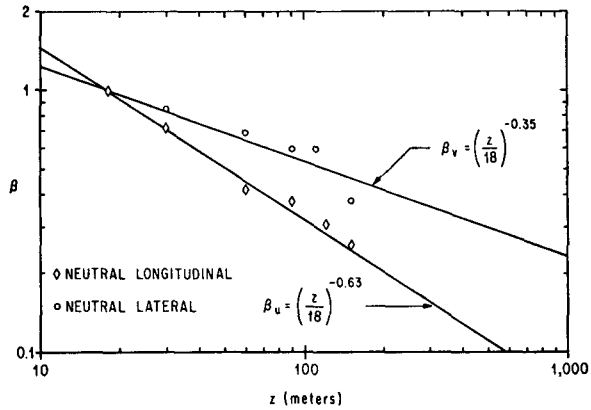

FIG. 10. Vertical distributions of the collapsing factors β_u and β_v for neutral stability conditions.

was selected to represent the longitudinal spectrum, where C_u and r_u are positive constants, determined by a least-squares analysis. For sufficiently small values of f, $nS_u(n)/\beta_u u_{*0}^2$ asymptotically behaves like f/f_{mu} which is the correct behavior for a one-dimensional spectrum. At large values of f, $nS_u(n)/\beta_u u_{*0}^2$ asymptotically behaves like $(f/f_{mu})^{-2/3}$, consistent with the concept of the inertial subrange. The maximum value of (33) occurs at $f=f_{mu}$. Various authors have suggested formulae like (33) to represent the longitudinal spectrum. However, most of the representations have only one adjustable parameter available, while (33) has two: C_u and r_u. In this light (33) appears to be superior. C_u controls the magnitude of the peak, r_u controls the peakedness, and f_{mu} determines the position of the peak of $nS_u(n)/u_{*0}^2$. Upon setting $r_u=5/3$, we obtain the form of the longitudinal spectrum suggested by Panofsky (1964) to represent the strong wind spectra of Davenport (1961). von Kármán's longitudinal spectrum (1961) can be obtained by setting $r_u=2$. A least-squares analysis of the longitudinal data in Fig. 11 revealed that $C_u=6.198$ and $r_u=0.845$.

The lateral spectra S_v can be collapsed with a procedure like the one used for the longitudinal spectra. However, to determine an analytical expression for the lateral spectrum, special attention must be paid to the inertial subrange to guarantee that $S_u/S_v=3/4$ (Batchelor, 1953). This requirement can be derived from the mass continuity equation for incompressible flow subject to the condition that the eddies are isotropic in the inertial subrange. The experimental values of f_{mu} and β_v are given in Figs. 9 and 10. These data show that f_{mv} and β_v can be represented as power laws as for the longitudinal spectra. The function

$$\frac{nS_v(n)}{\beta_v u_{*0}^2}=\frac{C_v f/f_{mv}}{[1+1.5(f/f_{mv})^{r_v}]^{5/3r_v}} \tag{34}$$

was used to represent the scaled spectra, where C_v and

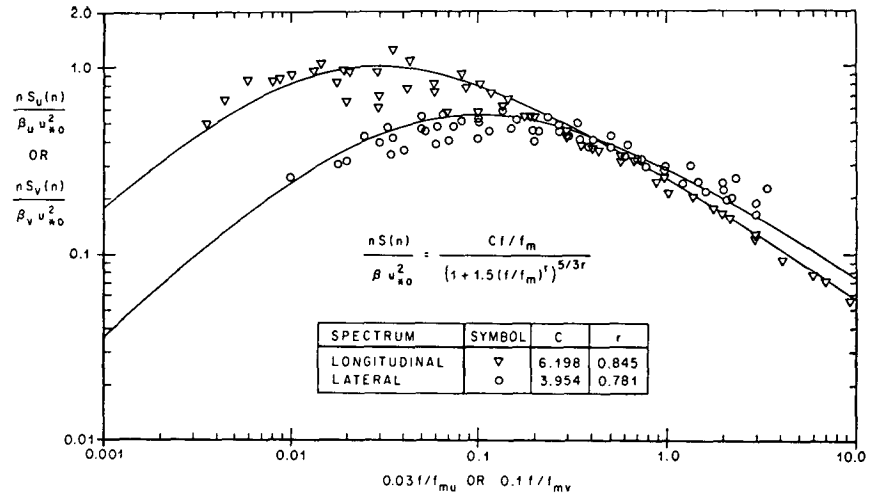

FIG. 11. Dimensionless logarithmic longitudinal and lateral spectra as functions of $0.03\ f/f_{mu}$ and $0.1\ f/f_{mv}$ for neutral stability conditions.

r_v are positive constants. This function behaves like the one chosen for the longitudinal spectrum.

For sufficiently large values of f, the asymptotic behavior of the ratio between (33) and (34) is given by

$$\frac{S_u}{S_v} \approx \frac{C_u}{C_v}\frac{\beta_u}{\beta_v}\left(\frac{f_{mu}}{f_{mv}}\right)^{\frac{2}{3}}\left(\frac{3}{2}\right)^{5/3(1/r_v-1/r_u)}. \tag{35}$$

In the inertial subrange we must have $S_u/S_v=3/4$, so that upon substituting this ratio into (35), we obtain a relationship that can be used as a constraint in the determination of values of C_v and r_v and functions to represent β_v and f_{mv}. The values $C_v=3.954$ and $r_v=0.781$, and the functions

$$f_{mv}=0.1(z/18)^{0.58}, \tag{36}$$

$$\beta_v=(z/18)^{0.35}, \tag{37}$$

along with the longitudinal parameters will satisfy condition (35) and simultaneously give a good fit to the data (z is in meters). The collapsed lateral spectra and the functions given by (33) and (34) are shown in Fig. 11.

6. Unstable spectra

To develop an engineering model for unstable conditions, the unstable spectra were averaged and then corrected by multiplication with

$$\left[\left(\ln\frac{z}{z_0}-\psi(\mathrm{Ri})\right)\Big/\left(\chi^{-1}\ln\frac{z}{z_0}-\psi(\mathrm{Ri})\right)\right]^2$$

for $z=18$ m, $z_0=0.18$ m and $\mathrm{Ri}=-0.3$. The longitudinal and lateral spectra for the mean unstable conditions are shown in Figs. 12 and 13. The unstable spectra were collapsed by using the procedures for the neutral boundary layer and the functions (33) and (34) appear to be equally valid for the unstable case. The functions f_{mu}, f_{mv}, β_u and β_v are depicted in Figs. 14 and 15 and the functions $nS_u(n)/\beta_u u_{*0}^2$ and $nS_v(n)/\beta_v u_{*0}^2$ are given

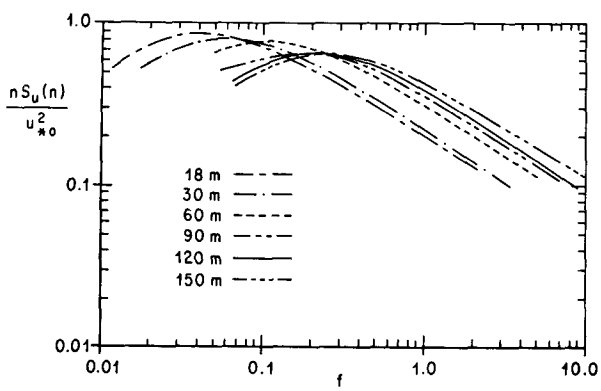

FIG. 12. Dimensionless logarithmic longitudinal spectra for unstable wind conditions.

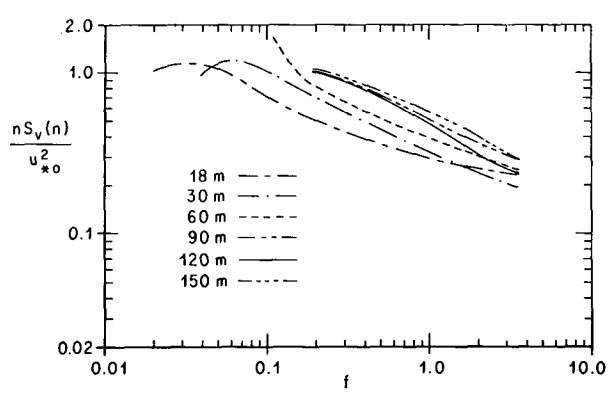

FIG. 13. Dimensionless logarithmic lateral spectra for unstable wind conditions.

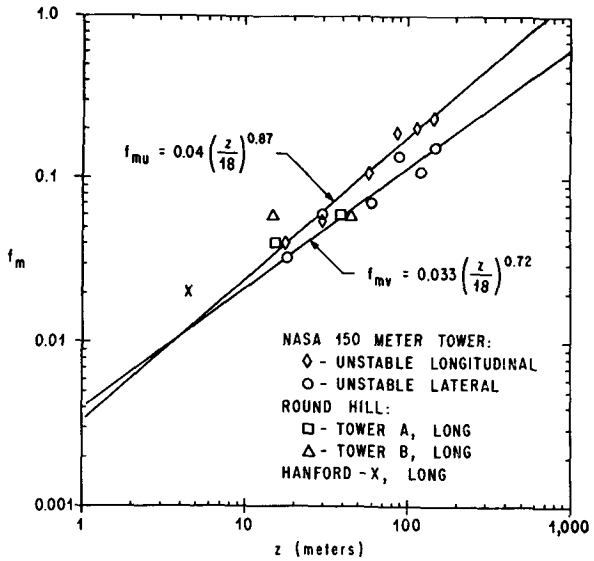

FIG. 14. Vertical distributions of the dimensionless frequencies f_{mu} and f_{mv} associated with the peaks of the logarithmic longitudinal and lateral spectra for unstable wind conditions.

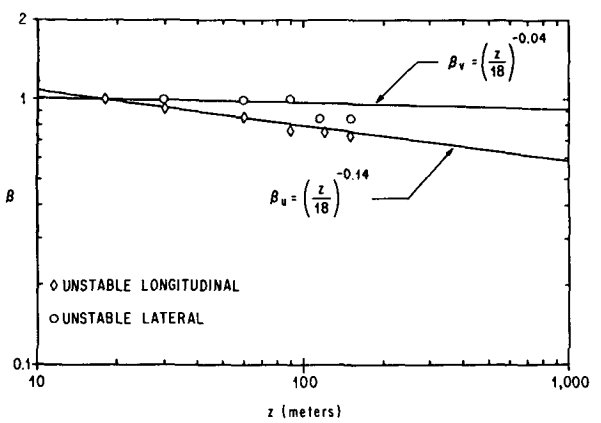

FIG. 15. Vertical distributions of the collapsing factors β_u and β_v for unstable wind conditions.

in Fig. 16. Table 1 summarizes the spectral properties of turbulence for unstable and neutral conditions.

7. The longitudinal and lateral correlation functions

The normalized correlation function $R(x)$ at space lag x is related to the spectrum through the Fourier integral

$$\sigma^2 R(x) = \bar{u} \int_0^\infty S(\bar{u}\kappa) \cos(2\pi\kappa x) d\kappa, \tag{38}$$

where $\bar{u}S(\bar{u}\kappa)$ is the spectrum at wavenumber κ (cycles m^{-1}) and σ is the standard deviation of the turbulence.

The wavenumber is related to the frequency through Taylor's hypothesis ($\kappa = n/\bar{u}$). Substitution of (33) or (34) into (38) yields

$$\frac{\sigma^2 R(\xi)}{\beta u_{*0}^2} = C \int_0^\infty \frac{\cos(2\pi\xi\zeta) d\zeta}{(1+1.5\zeta^r)^{5/3r}}, \tag{39}$$

where

$$\left.\begin{aligned} \zeta &= f/f_m \\ \xi &= x f_m / z \end{aligned}\right\}. \tag{40}$$

The quantity ξ is the dimensionless space lag at height z and the integral in (39) is a function of ξ only. Integration of (39) for neutral and unstable conditions with Simpson's rule yielded the results shown in Figs. 17 and 18.

The dimensionless standard deviation $\sigma/\beta^{1/2}u_{*0}$ can be obtained from (39) by setting $\xi = 0$ and then taking the

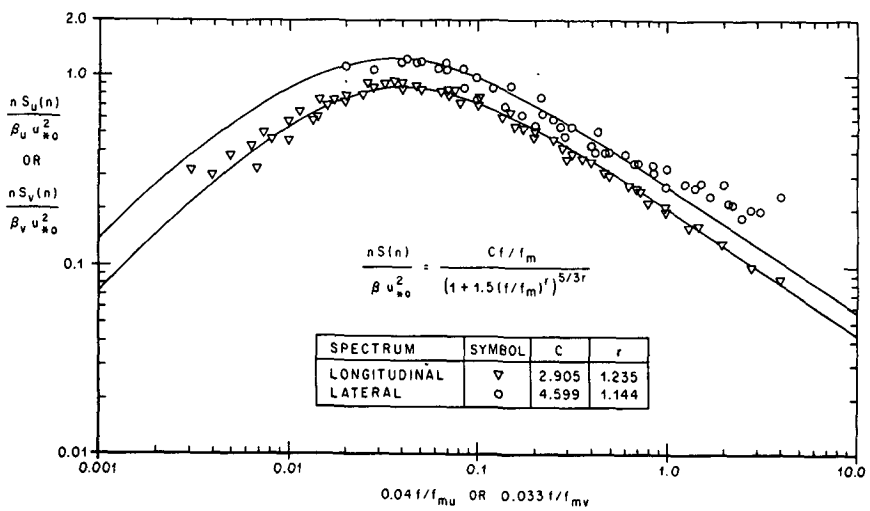

FIG. 16. Dimensionless logarithmic longitudinal and lateral spectra as functions of $0.04\ f/f_{mu}$ and $0.033\ f/f_{mv}$ for unstable wind conditions.

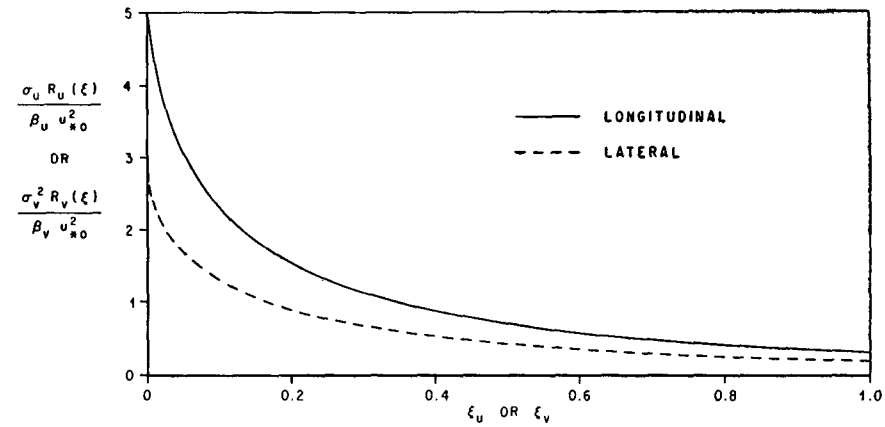

FIG. 17. Scaled correlation functions for the longitudinal and lateral components of turbulence as functions of the dimensionless space lag ξ for neutral wind conditions.

positive square root of the resulting expression, so that

$$\frac{\sigma}{\beta^{\frac{1}{2}}u_{*0}}=\left[C\int_0^\infty \frac{d\zeta}{(1+1.5\zeta^r)^{5/3r}}\right]^{\frac{1}{2}}. \tag{41}$$

The right-hand side of (41) is a pure number, values for which can be found in Table 2.

The function

$$\frac{\sigma^2R(\xi)}{\beta u_{*0}^2}=\frac{\sigma^2}{\beta u_{*0}^2}\left[1+\frac{6.815}{\delta}\frac{C}{(1.5)^{5/3r}}\frac{\beta u_{*0}^2}{\sigma^2}\xi^{\frac{2}{3}}\right]^{-\delta}, \tag{42}$$

was selected to represent the results of the numerical integrations for the neutral case. The parameter δ is determined by least-squares methods. For sufficiently small values of ξ, this function behaves like

$$R(\xi)=1-6.815\left[\frac{C}{(1.5)^{5/3r}}\right]\frac{\beta u_{*0}^2}{\sigma^2}\xi^{\frac{2}{3}}. \tag{43}$$

Now the theory of isotropic homogeneous turbulence predicts that in the inertial subrange

$$\frac{R_v(x)-1}{R_u(x)-1}=\frac{4}{3}, \tag{44}$$

and (43) predicts that

$$\frac{R_v(x)-1}{R_u(x)-1}\rightarrow\left[\frac{C_v}{C_u}\frac{\beta_v}{\beta_u}\left(\frac{f_{mv}}{f_{mu}}\right)^{\frac{2}{3}}\left(\frac{3}{2}\right)^{5/3(1/r_u-1/r_v)}\right]\left(\frac{\sigma_u}{\sigma_v}\right)^2, \tag{45}$$

as $\xi\rightarrow 0$. The quantity within the brackets on the right-hand side of (45) is equal to 4/3, and $\sigma_u/\sigma_v\neq 1$. The apparent inconsistency between (44) and (45) results because (44) is based upon the entire flow being isotropic, while (45) is based on spectra associated with turbulent flows which are only locally isotropic in wavenumber space for sufficiently large wavenumbers. Thus, upon producing the Fourier integral, Eq. (39), we obtained contributions to $R(\xi)$ from both the isotropic and anisotropic portions of the turbulent flow. The quantities $\delta_u=4.758$ and $\delta f=3.399$ and the function (42) reproduce the results of the numerical integrations of (39), for the neutral case, to within a few per cent.

In the unstable case, the function (42) does not reproduce the results of the numerical integrations at large values of ξ. To remedy this, an exponential factor was introducted into the expression, and the function

$$\frac{\sigma^2R(\xi)}{\beta u_{*0}^2}=\frac{\sigma^2}{\beta u_{*0}^2}\left[1+6.815\frac{C}{(1.5)^{5/3r}}\frac{\beta u_{*0}^2}{\sigma^2}\xi^{\frac{2}{3}}\right]^{-1}e^{-\lambda\xi^\gamma} \tag{46}$$

was selected to represent the results of numerical integrations for the unstable case. The quantities λ and γ are determined by least-squares methods. It appears that $\gamma=0.9$ can be used for both the longi-

TABLE 1. Summary of the spectral properties of turbulence for neutral and unstable conditions.

$$\frac{nS(n)}{\beta u_{*0}^2}=\frac{Cf/f_m}{[1+1.5(f/f_m)^r]^{5/3r}}$$

	Neutral	Unstable
C_u	6.198	2.905
C_v	3.954	4.599
r_u	0.845	1.235
r_v	0.781	1.144
f_{mu}	$0.03(z/18)$	$0.04(z/18)^{0.87}$
f_{mv}	$0.1(z/18)^{0.58}$	$0.033(z/18)^{0.72}$
β_u	$(z/18)^{-0.63}$	$(z/18)^{-0.14}$
β_v	$(z/18)^{-0.35}$	$(z/18)^{-0.04}$

TABLE 2. Table of properties of the correlation functions for neutral and unstable conditions.

	Neutral	Unstable
$\sigma_u/(\beta_u^{\frac{1}{2}}u_{*0})$	2.227	1.897
$\sigma_v/(\beta_v^{\frac{1}{2}}u_{*0})$	1.677	2.302
$L_u{}^*f_{mu}/z$	0.282	0.188
$L_v{}^*f_{mv}/z$	0.332	0.199

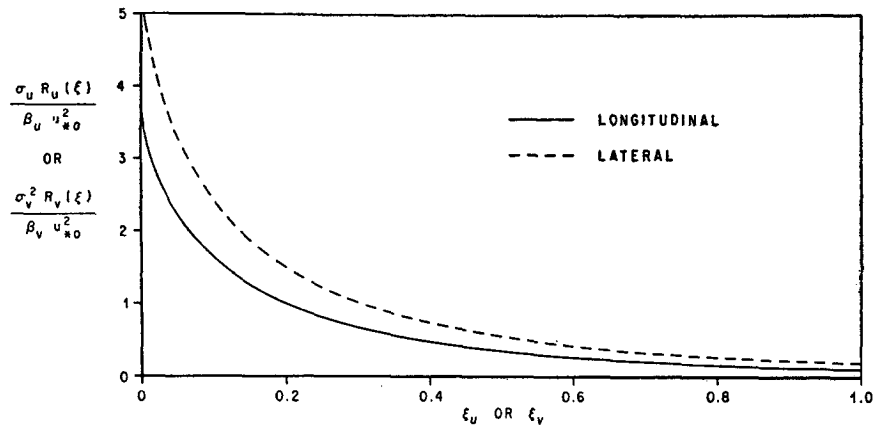

FIG. 18. Scaled correlation functions for the longitudinal and lateral components of turbulence as functions of the dimensionless space lag ξ for unstable wind conditions.

tudinal and lateral spectra, and

$$\left.\begin{aligned}\lambda_u&=2.22\\ \lambda_v&=2.02\end{aligned}\right\}.$$

The function (46) yields a good fit near $\xi=0$; however, it departs from the results of the numerical integrations by $\sim 10\%$ at $\xi=1$. Near the origin, (46) behaves like (43), consistent with hypothesis of the inertial subrange.

Let us now turn our attention to the longitudinal and lateral scales of turbulence which are defined by the expression

$$L^*=\int_0^\infty R(x)dx. \tag{47}$$

The integral scale defined in terms of the dimensionless space lag is given by

$$\frac{L^* f_m}{z}=\int_0^\infty R(\xi)d\xi. \tag{48}$$

This integral is a pure number, and upon substituting the expressions given by (42) and (46) for $R(\xi)$ and employing Simpson's integration rule, we obtain the results in Table 2.

Pasquill (1962) has represented the correlation functions of atmospheric turbulence with the expression

$$R(x)=e^{-x/L^*}. \tag{49}$$

The logarithmic spectrum associated with this expression is given by

$$\frac{nS(n)}{u_{*0}^2}=\frac{2}{\pi}\frac{\sigma^2}{u_{*0}^2}\left[\frac{2\pi fL^*/z}{(2\pi fL^*/z)^2+1}\right]. \tag{50}$$

This function has a maximum value at

$$\frac{L^* f_m}{z}=\frac{1}{2\pi}=0.159. \tag{51}$$

This value of the dimensionless integral scale is significantly less ($\sim 45\%$) than the ones in Table 2 for the neutral case. However, for the unstable case, the integral scales given by (51) depart from the ones in Table 2 by only $\sim 20\%$.

In the neutral case, f_{mu} and f_{mv} are proportional to z and $z^{0.58}$, so that L_u^* is a constant and $L_v^* \propto z^{0.42}$. The former is consistent with the results of Davenport's (1961) analysis of high wind speed spectra. In unstable air, f_{mu} and f_{mv} are proportional to $z^{0.87}$ and $z^{0.72}$, and thus L_u^* and L_v^* are proportional to $z^{0.13}$ and $z^{0.28}$.

8. The dissipation rate of turbulence

It is possible to estimate the dissipation rate of turbulence by examining the asymptote of the dimensionless logarithmic spectrum for large f values. According to (33), the longitudinal spectrum, for sufficiently large values of f, is asymptotically given by

$$\frac{nS_u(n)}{u_{*0}}\approx\beta_u\left[\frac{C_u}{(1.5)^{5/3r_u}}\right](f/f_{mu})^{-\frac{2}{3}}. \tag{52}$$

Equating the right-hand sides of (13) and (52), we obtain

$$\phi_\epsilon=\left[\frac{k_1}{(1.5)^{5/2r_u}}\right](C_u/\alpha)^{\frac{3}{2}}\beta_u^{\frac{3}{2}}f_{mu}. \tag{53}$$

According to the information given in Table 1 and (53), ϕ_ϵ in neutral air is given by

$$\phi_\epsilon=(z/18)^{0.055}, \tag{54}$$

while in unstable air, we have

$$\phi_\epsilon=0.63(z/18)^{0.66}. \tag{55}$$

One should keep in mind that (55) was derived from a spectral model which is an average of the unstable spectra, so that (55) is probably valid for conditions associated with values of Ri approximately equal to -0.3.

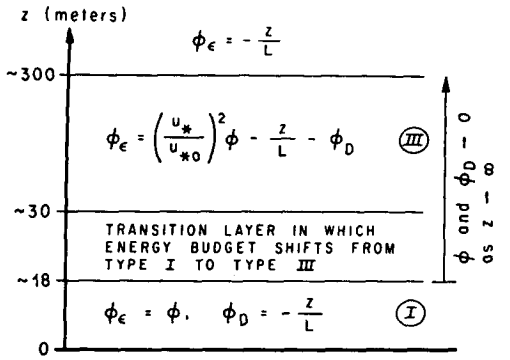

FIG. 19. Hypothesized scheme of the budget of turbulent energy in the unstable boundary layer for Ri(18 m)≈ -0.3.

At $z/L=0$ we have $\phi(0)=1$, so that according to either hypothesis I or II [see (19) or (21)], we must have $\phi_\epsilon(0)=1$. However, (54) predicts that $\phi_\epsilon(0)<1$ below $z=18$ m for the neutral case and at $z=0$ we have $\phi_\epsilon(0)=0$. Actually, the layer of air in the domain $0<z\leqq 18$ m is in the Monin layer, and we should have $\phi_\epsilon=1$ throughout this layer during neutral conditions. If we accept a 10% error in ϕ_ϵ as a measure of the validity of the spectral representations given by (33) and (34), then it follows from (54) that the model can be extrapolated down to the 3-m level in the neutral case.

To understand the behavior of ϕ_ϵ in the unstable case, we write the eddy energy equation for the steady state boundary layer in the form

$$(u_*/u_{*0})^2\phi-\frac{z}{L}-\phi_\epsilon-\phi_D=0. \tag{56}$$

Let us now assume that the heat flux is height invariant, so that L is a constant. At the surface of the earth z/L vanishes, $(u_*/u_{*0})^2\phi(0)=1$, and $\phi_D(0)=0$, according to both hypotheses I and II; thus, $\phi_\epsilon(0)=1$. As we proceed away from the earth into the unstable Monin layer, ϕ_D is balanced by z/L and ϕ_ϵ is balanced by ϕ according to hypothesis I (in the Monin layer, $u^*=u_{*0}$). Because ϕ is a decreasing function of $-z/L$, it follows that ϕ_ϵ is a decreasing function of z for $z<18$ m. However, using an analysis of a sample of Cape Kennedy data, Panofsky (see Blackadar *et al.*, 1969) suggests that ϕ_D is unimportant in unstable air at 30 m and above. This conclusion may not be strictly true for the entire layer above 30 m, but it is reasonable to suppose ϕ_D becomes negligibly small or vanishes somewhere above 30 m. In addition, for sufficiently large z, the dimensionless shear ϕ is small compared to $-z/L$ and $(u^*/u_{*0})^2<1$, so that, according to (56), ϕ_ϵ can be estimated as $-z/L$. Thus, at sufficiently large heights, ϕ_ϵ is an increasing function of z. Therefore, ϕ_ϵ must experience a minimum in the lower levels. Eq. (55) implies that ϕ_ϵ is an increasing function of z in the unstable boundary layer [Ri(18 m)≈ -0.3] for $z\geqq 18$ m, and thus (55) and hypothesis I predicts that the minimum in ϕ_ϵ occurs at the 18 m level. This result is nonsense and can be attributed to the fact that the spectra at the various heights were standardized in terms of the 18 m spectra. Nevertheless, if the implications of hypothesis I are correct, the minimum in ϕ_ϵ should occur somewhere below the 18-m level for 18-m Richardson numbers on the order of -0.3. If this minimum in ϕ_ϵ exists, it was not detected because of the wide spacing between the instrumentation levels on the tower and the scatter of the data.

The level above 30 m at which ϕ_D vanishes in the unstable model can be estimated with (56). Following Blackadar *et al.* (1969), we assume $(u_*/u_{*0})^2\phi$ is small compared to $-z/L$, set $\phi_D=0$ in (56), and combine the resulting relationship with (55) to yield

$$\frac{z^*}{L}=0.63(z^*/18)^{0.66}, \tag{57}$$

where z^* is the level at which ϕ_D vanishes. The 18-m level Richardson number for the mean unstable model is on the order of -0.3. Therefore, according to (6), $18/L'=-0.19$. Now, $L=K_mL'/K_h$ and $K_h/K_m\approx 1.3$, so that $L=-73$ m. Substituting this value of L into (57) yields $z^*=283$ m. Above this level, ϕ and ϕ_D are small, and $\phi_\epsilon\approx -z/L$. This should be compared with (55) which predicts ϕ_ϵ increases as $z^{0.66}$.

9. Concluding comments

An engineering model of the longitudinal and lateral spectra of turbulence has been developed. The analytical expressions used to represent the spectra are asymptotically consistent at sufficiently large wavenumbers with the well-known properties of isotropic turbulence in the inertial subrange. Based on an analysis of the longitudinal spectrum in the inertial subrange at the 18-m level it seems that in the Monin layer the mechanical and buoyant production rates of turbulent kinetic energy are balanced by the viscous dissipation and flux divergence terms, respectively. However, since the friction velocity was not measured directly, it is not possible to be sure that the correct hypothesis of the energy budget has really been selected. The friction velocities are derived for these cases from mean wind speed and temperature profiles by the use of assumptions whose validity can only be established if the friction velocity is known. Accordingly, the proposed energy budget should be considered tentative.

The Fourier transform mates, or rather the correlation functions associated with the spectral representations, were obtained by numerical integration and formulae were selected to represent the results of these integrations. It is concluded from an analysis of the correlation functions that σ_u and σ_v behave as $z^{-0.315}$ and $z^{-0.175}$ in neutral air, while in unstable air they are proportional to $z^{-0.07}$ and $z^{-0.02}$. In neutral air the longitudinal integral scale of turbulence is height invariant, while the lateral integral scale behaves as $z^{-0.42}$. In unstable air L_u^* and L_v^* are proportional to $z^{-0.13}$ and $z^{-0.28}$.

The vertical variation of the viscous dissipation was deduced from the spectral model. In the neutral boundary layer $\phi_\epsilon \propto$ to $z^{0.055}$, so that $\epsilon \propto z^{-0.945}$. In the unstable boundary layer $\phi_\epsilon \propto z^{0.66}$, so that $\epsilon \propto z^{-0.34}$.

As one proceeds upward out of the Monin layer, the energy balance seems to become more complex, because the selective energy balance that occurs in the Monin layer fails in the Ekman layer and thus the mechanical and buoyant production terms together balance the viscous dissipation and flux divergence terms. At sufficiently great heights on the order of 300 m, it seems that we again have a selective energy balance; however, we now have a situation in which the mechanical production and flux divergence terms are small and the buoyant production is balanced by the viscous dissipation.

It should be kept in mind that the statistics of horizontal velocity fluctuations are functions of the surface roughness in the immediate vicinity of the site, as well as the distributions of surface roughness and obstructions (buildings, trees, etc.) within a radius of approximately 100 km from the site. In this light one should proceed cautiously when applying the model contained herein to other sites.

The proposed energy budget scheme for the unstable boundary layer is summarized in Fig. 19. In the lowest layer, the Monin layer, the energy budget is given by hypothesis I [see (19)]. Above this layer, there is a transition region, between approximately the 18- and 30-m levels, in which the energy budget transforms from a type I to a type III budget. A type III budget is one in which the mechanical and buoyant energy production terms and the energy flux divergence term all contribute to balance ϕ_ϵ to varying degrees. From the base of the transition layer to a level on the order of 300 m, ϕ and ϕ_D tend toward zero as z increases. Finally, above this level we have a region in which the buoyant energy production is balanced by the dissipation. In order for this scheme to work, the various functions in the energy equation must be functions of z/L and z scaled with a length scale other than L. The additional length scale should be a function of the external synoptic and mesoscale conditions which force the turbulent flow in the boundary layer.

Acknowledgments. The authors are grateful to Prof. Hans A. Panofsky for the discussions and suggestions during the course of this research. The authors wish to thank Mr. Archie Jackson and Mrs. Ella M. McAllister of the Marshall Space Flight Center Computation Laboratory for performing the programming and necessary computations, and Mrs. Margaret B. Alexander, Mr. Julian Nelson and Mr. Douglas Mackiernan of the Atmospheric Dynamics Branch, Marshall Space Flight Center, for their assistance in completing this paper.

REFERENCES

Batchelor, G. K., 1953: *The Theory of Homogeneous Turbulence.* New York, Cambridge Univ. Press, 197 pp.

Berman, S., 1965: Estimating the longitudinal wind spectrum near the ground. *Quart. J. Roy. Meteor. Soc.*, **91**, 302–317.

Blackadar, A. K., *et al.*, 1965: Flux of heat and momentum in the planetary boundary layer of the atmosphere. The Pennsylvania State University, Mineral Industries Experiment Station, Dept. of Meteorology, Contract AFCRL No. AF9604-6641, 140 pp.

——, J. A. Dutton, H. A. Panofsky and A. Chaplin, 1969: Investigation of the turbulence wind field below 500 feet altitude at the Eastern Test Range, Florida. NASA CR-1410, National Aeronautics and Space Administration, Washington, D. C., 92 pp.

Blackman, R. B., and J. W. Tukey, 1958: *The Measurement of Power Spectra.* New York, Dover Publ., 190 pp.

Busch, N. E., and H. A. Panofsky, 1968: Recent spectra of atmospheric turbulence. *Quart. J. Roy. Meteor. Soc.*, **94**, 132–148.

Davenport, A. G., 1961: The spectrum of horizontal gustiness near the ground in high winds. *Quart. J. Roy. Meteor. Soc.*, **87**, 194–211.

Fichtl, G. H., 1968: Characteristics of turbulence observed at the NASA 150-m meteorological tower. *J. Appl. Meteor.*, **7**, 838–844.

Kaufman, J. W., and L. F. Keene, 1965: NASA's 150-meter meteorological tower located at Cape Kennedy, Florida. NASA TM-X-53259, George C. Marshall Space Flight Center, Huntsville, Ala.

Lumley, J. L., and H. A. Panofsky, 1964: *The Structure of Atmospheric Turbulence.* New York, Interscience Publ. and Wiley & Sons, 239 pp.

Monin, A. S., 1959: On the similarity of turbulence in the presence of a mean vertical temperature gradient. *J. Geophys. Res.*, **64**, 2196–2197.

Pasquill, F., 1962: *Atmospheric Diffusion.* New York, van Nostrand, 297 pp.

Record, F. A., and H. E. Cramer, 1966: Turbulent energy dissipation rates and exchange processes above a non-homogeneous surface. *Quart. J. Roy. Meteor. Soc.*, **92**, 519–532.

von Kármán, T., 1961: Progress in the statistical theory of turbulence. *Turbulence-Classic Papers on Statistical Theory*, New York, Interscience, 162–174.